The magnetization of epitaxial nanometric CoFe 2 O 4 (001) layers

F. Rigato, J. Geshev, V. Skumryev, and J. Fontcuberta

Citation: Journal of Applied Physics **106**, 113924 (2009); doi: 10.1063/1.3267873
View online: http://dx.doi.org/10.1063/1.3267873
View Table of Contents: http://scitation.aip.org/content/aip/journal/jap/106/11?ver=pdfcov
Published by the AIP Publishing

The magnetization of epitaxial nanometric $CoFe_2O_4$(001) layers

F. Rigato,[1,a)] J. Geshev,[2] V. Skumryev,[3] and J. Fontcuberta[1]
[1]*Institut de Ciència de Materials de Barcelona (ICMAB-CSIC), Campus UAB s/n, 08193 Bellaterra, Spain*
[2]*Instituto de Física, Universidade Federal do Rio Grande do Sul (UFRGS), Porto Alegre, 91501-970 Rio Grande do Sul, Brazil*
[3]*Institut Català de Recerca i Estudis Avançats (ICREA), and Departament de Física, Universitat Autònoma de Barcelona, 08193 Bellaterra, Spain*

(Received 23 September 2009; accepted 29 October 2009; published online 15 December 2009)

We have studied the magnetic anisotropy of nanometric $CoFe_2O_4$ (CFO) thin films grown on (100)$SrTiO_3$ (STO) substrates. It has been found that epitaxial substrate-induced compressive strain makes the normal-to-film axis harder than the in-plane directions. In agreement with some previous reports, the magnetization loops are found to display a characteristic shrinking at low fields. Detailed structural and microstructural analyses, together with a modeling of the magnetization loops, revealed that the microstructure of the films, namely, the coexistence of a continuous CFO and a distribution of pyramidal CFO huts emerging from the surface, are responsible for this peculiar feature. We argue that this behavior, which significantly impacts the magnetic properties, could be a general trend of spinel films grow on (001)STO substrates. © *2009 American Institute of Physics*. [doi:10.1063/1.3267873]

I. INTRODUCTION

In recent years, (ferri)magnetic spinel insulating oxides, such as $NiFe_2O_4$ or $CoFe_2O_4$ (CFO), have received much attention due to their potential use in advanced spintronic devices such as spin filters[1–5] or in multiferroic actuators.[6] Some of these applications require growth of epitaxial layers of these materials on suitable substrates, with sharp interfaces with substrates and bottom or upper layers. Sharp interfaces are particularly relevant in most demanding applications, where electronic coupling through interfaces is symmetry-controlled or where interface microstructure may determine the fine details of the magnetization process of the ferromagnetic layer. The magnetization processes in thin films are first determined by the balance of the magnetocrystalline (K_{mc}), the magnetoelastic (K_{me}), and the magnetostatic anisotropies, as well as the Zeeman energy. In addition, in ultrathin films the surface anisotropy (K_S) can be of relevance. CFO is quite unique among the spinels as its first-order magnetocrystalline anisotropy constant ($K_1>0$) is about one order of magnitude larger than that of other spinels due to lifting of degeneracy of the ground state [$3d^7$ states (Co^{2+})] as a response to the partial filling of the octahedral crystal-field states. The reported large magnetostriction (λ) of CFO is another manifestation of the same physics.

As a result of this subtle energy competition, it has been found that epitaxial CFO films display an easy-magnetization plane when grown in-plane compressively strained, as in the case of CFO on $SrTiO_3$ (STO),[7–9] whereas an easy-axis direction perpendicular to the plane is favored when grown under in-plane tensile strain.[10–13] These results are both compatible with the reported negative magnetostriction constant $\lambda_{[100]}<0$. On the other hand, it has been claimed that the antiphase boundaries (APBs) are the origin of the reduced magnetization and differential susceptibility quite often observed in ferrimagnetic spinel thin films.[14] However, beyond this broad agreement, some more intricate results remain to be elucidated. For instance, the recent observation of a spin reorientation from out-of-plane to in-plane type of anisotropy that takes place when increasing the thickness of CFO films grown on MgO has been interpreted as due to the dominating role of lattice strain.[13] Other than this, quite often the hysteresis loops of CFO thin films display an unexpected shrinking at low fields,[8–10,14] which although being of relevance for any practical application of CFO-based devices, has remained unexplained.

Recognizing the relevance of interfacial structure, recent reports[14] have shown that the composition of CFO films grown by molecular beam epitaxy (MBE) on (001)STO is preserved across the film thickness but not in an interface layer about 1 nm thick. Maybe of even higher relevance is the observation that when growing CFO (and other spinels) on cubic (001) perovskite substrates such as (001)STO, the exposed growing layer of CFO is the (001)-oriented one; however, the surface energy of the (001) planes of CFO is substantially larger that that of the (111) planes, as easily recognized by the octahedral habit of most spinel crystals. These observations are pertinent as they suggest that obtaining atomically flat (001) surfaces of CFO on (001)STO substrates is challenging and thus surface microstructure plays a significant role in determining the magnetic properties.

It is the purpose of this manuscript to analyze the magnetization of CFO thin films, epitaxially grown on STO, as a function of the films' thickness. We will show that the magnetization is determined not only by the magnetocrystalline anisotropy, the magnetoelastic and the magnetostatic contributions, and the Zeeman energy contribution described above, the surface anisotropy playing only a minor role, but also by the microstructure of the films' surface that becomes gradually more important when reducing the films' thickness.

[a)]Electronic mail: frigato@icmab.es.

We will show that the magnetization, and more precisely the low-field shrinking in the hysteresis loops, can be described as a superposition of contributions from the bulk of the (001)-epitaxial film and from arrays of pyramidal huts, which emerge from the film surface. Using appropriate modeling tools, the magnetization loops can be quantitatively described and the extracted anisotropy constants compared to those derived from structural and microstructural data.

II. EXPERIMENTAL

The cobalt ferrite layers with thicknesses (t) from 3.5 up to 50 nm were grown by radiofrequency magnetron sputtering in a mixed atmosphere of argon and oxygen (ratio 10:1), with a total pressure of 250 mTorr. The substrates, (001)-oriented STO single crystals, were maintained at 600 °C during the deposition and the growth rate was set at ≈0.12 nm/min.

Siemens D-5000 diffractometer and Cu Kα radiation were used for structural and thickness analyses. Film thickness was determined by x-ray reflectivity for the thicker films; for $t<10$ nm, the corresponding values were extrapolated from a calibration curve. X-ray diffraction reciprocal space maps were acquired by means of Advance D8 Bruker diffractometer with four-angle goniometer and area detector.

Magnetic characterization was performed at 10 K, using a Quantum Design superconducting quantum interference device (SQUID). The as obtained $M(H)$ curves have been corrected by subtracting the diamagnetic contribution of the substrate, estimated from the linear high-field slope of the raw data. We note that this experimental approach could underestimate the film magnetization as any eventual high-field susceptibility is included in the substrate contribution. However, the value of the high-field slope of the raw $M(H)$ data is very similar for all films $[(-4.55\pm0.81)\times10^{-7}$ emu Oe^{-1} cm$^{-3}]$ and it is in a good agreement with the measured susceptibility of a bare $SrTiO_3$ substrate $(-5.15\times10^{-7}$ emu Oe^{-1} cm$^{-3})$, thus indicating full saturation of the film. The $M(H)$ curves have been corrected for demagnetization effect.[15]

Surface imaging and topography studies were performed by means of atomic force microscopy (AFM) and field emission scanning electron microscopy (FE-SEM).

III. RESULTS AND DISCUSSION

We first show in Fig. 1(a) the low-temperature (10 K) magnetization loop of a CFO‖(001)STO film (t=13.4 nm) measured with H parallel and perpendicular to plane of the film. Inspection of these data clearly indicates that the in-plane direction is easier than the out-of-plane one, in agreement with previous results of CFO on STO.[8–10] The in-plane biaxial anisotropy results from a compressive in-plane strain epitaxially induced by the STO substrate (see below) and a negative magnetostriction constant. The magnetization loops, measured with H applied in plane at different angles with respect to the [100] direction, do not display significant anisotropy [Fig. 1(b)].

Figure 2 shows the magnetization loops of CFO films of various thicknesses (t=3.5, 6.5, 10.8, and 41.7 nm), measured with H in plane, applied along the [100] direction. The data in this figure display two streaking features: (a) the saturation magnetization (M_S) of the CFO is not a constant but gradually decreases with decreasing thickness, and (b) the hysteresis loops present a characteristic shrinking at low fields and a progressive enhancement of the coercive field with the thickness. Below we discuss these experimental results in the same order.

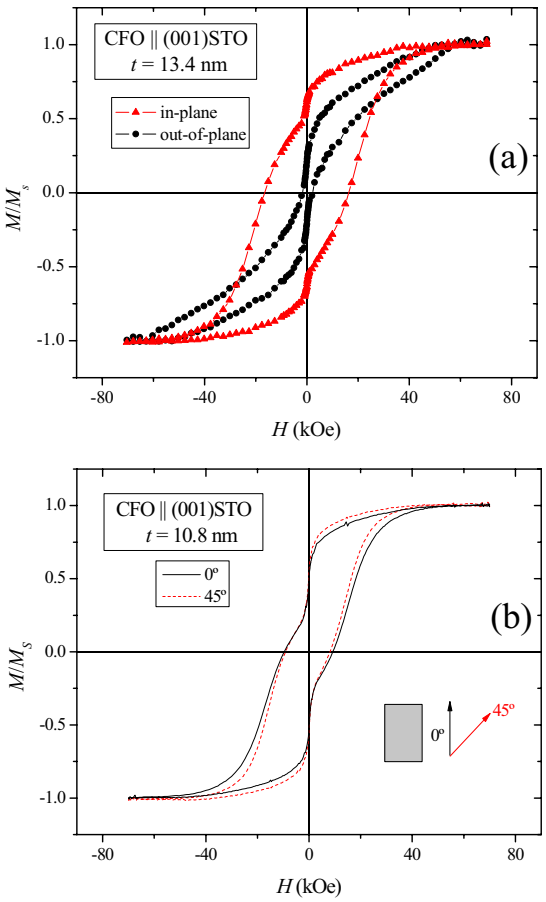

FIG. 1. (Color online) Magnetization curves at 10 K of $CoFe_2O_4$ films with the magnetic field applied (a) in-plane and perpendicular out-of-plane (t =13.4 nm), and (b) in-plane along two different angles with respect to the [100] direction (t=10.8 nm).

It is found from Fig. 2 that M_S decreases from 523 emu/cm^3 for t=3.5 nm to 255 emu/cm^3 for t =41.7 nm. The observation of a reduced saturation magnetization in spinel thin films, as compared to its bulk form, has been repeatedly reported and it has been attributed to the presence of antiphase boundaries.[16] More striking is the enhanced magnetization observed for the thinnest films. Similar behavior has also been reported for $NiFe_2O_4$ and attributed to partial inverse cationic distribution $(Fe_{1-x}Ni_x)\times[Fe_{1+x}Ni_{1-x}]O_4$ over octahedral and tetrahedral sites of the spinel structure.[17]

In the context of the present manuscript, of major interest is to elucidate the origin of the shrinking of the $M(H)$ loops, particularly noticeable for the thinnest films in Fig. 2. This feature, already mentioned in the Introduction, can also be observed in data reported earlier (see, for instance, Refs. 8–10 or Ref. 14) and has remained so far unexplained. The $M(H)$ loops present a clear two-steps behavior, with the

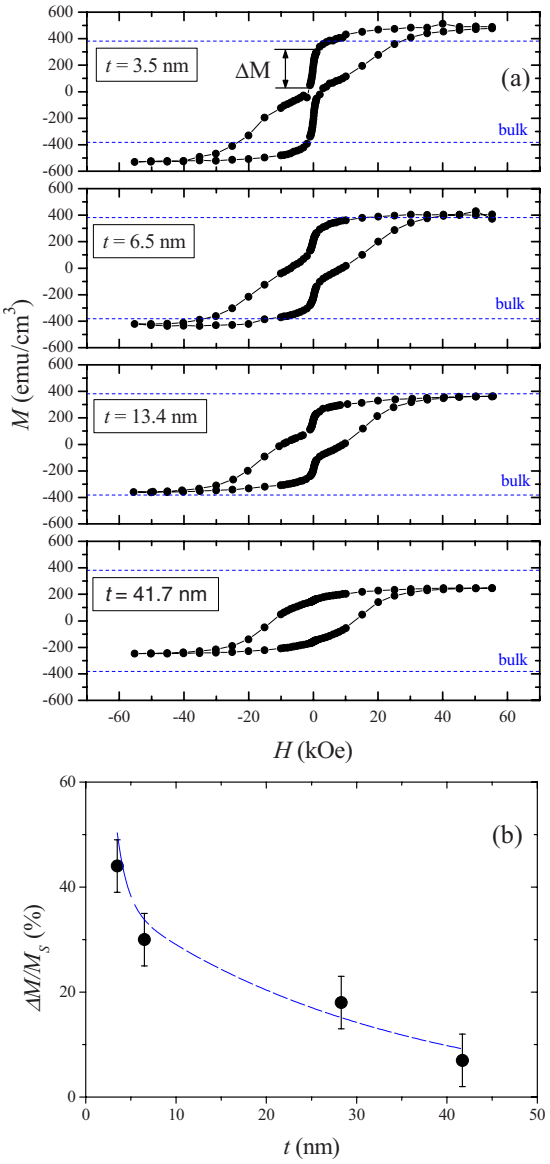

FIG. 2. (Color online) (a) Magnetization curves at 10 K of $CoFe_2O_4$ films of various thicknesses. The magnetic field is applied along [100]. The dashed lines indicate the values of CFO bulk magnetization. (b) Relative intensity of the magnetization drop with respect to the total magnetization as a function of film thickness (the lines are guides to the eyes).

magnetization sharply decreasing (ΔM) at a small return field. In Fig. 2(b), we show the thickness dependence of the relative amplitude $\Delta M/M_S$ of the jump of magnetization. The experimental observation that this double-step structure is washed out for the thicker films can be viewed as a signature of the presence of two different "magnetic phases," say, A and B, whose relative contributions are thickness dependent. The gradual increase in the coercive field with the thickness, achieving values of about 17 kOe for t=41.7 nm, would also be consistent with the presence of a soft and a hard magnetic phase in the films. Moreover, a detailed inspection of the shape of the M versus H loops reveals that they become sheared when increasing thickness. This would also indicate that epitaxial-induced strain has an impact on the shape of the magnetization loops.

To address these issues, in the following we report detailed structural and microstructural characterizations of the

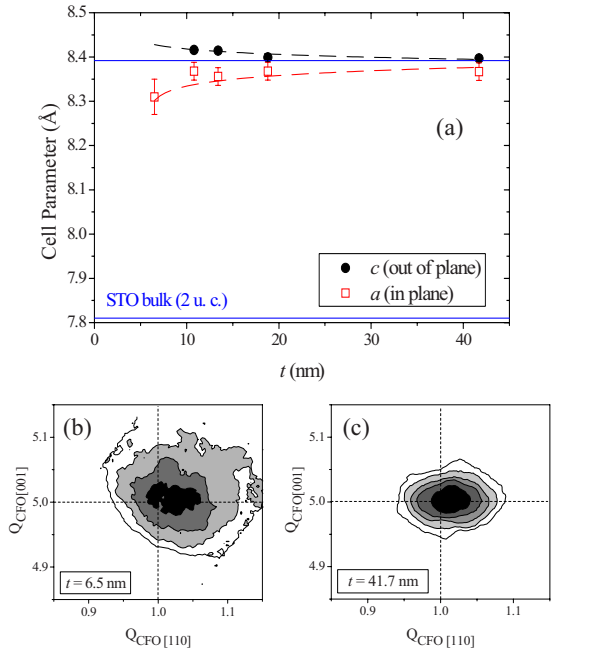

FIG. 3. (Color online) (a) Thickness dependence of the in-plane (squares) and out-of-plane (circles) cell parameters of CFO films (the dashed lines are guides to the eyes); (b) and (c) are the reciprocal space maps around the (115) reflection of CFO films of thicknesses 6.5 and 41.7 nm, respectively. The dashed lines indicate the position of bulk (115) CFO reflections.

films. It will be shown that indeed the thinnest films are in-plane compressively strained and the strain is progressively relaxed when increasing film thickness. Importantly, inspection of surface morphology by AFM and FE-SEM revealed the presence of a network of pyramidal huts and we will show that they dominate the magnetization loops of the thinnest films.

Reciprocal space maps and θ-2θ x-ray diffraction scans have been used to determine the in-plane and out-of-plane cell parameters of all films [Fig. 3(a)] and the epitaxial relationships. It turns out that, in agreement with previous results,[7,14] CFO grows cube on cube on STO, c-axis textured and [100]CFO∥[100]STO. No traces of other spurious phases could be detected by x-ray diffraction. In Figs. 3(b) and 3(c), we show illustrative examples of the reciprocal space maps around the (115) reflection of the CFO for the films with t=6.5 and 41.7 nm. It turns out [Fig. 3(a)] that the in-plane cell parameter (a) of the CFO films [squares in Fig. 3(a)] differs significantly from that of the substrate (the bulk cell parameter is 8.392 Å), indicating a substantial structural relaxation due to the large mismatch between the cell parameters of the STO and those of CFO (≈7.4%, calculated for two STO unit cells). In fact, one notices that the in-plane parameters of the thinner CFO films are smaller than that of bulk CFO thus indicating the presence of a residual compressive strain in the basal plane. In agreement with this observation, the out-of-plane parameter (c) [circles in Fig. 3(a)] of the thinner CFO films is expanded with respect to the bulk CFO. Therefore, $(a-c)/a<0$. It is clear from the data in Fig. 3(a) that there is a gradual strain relaxation when increasing the thickness.

The morphology of the film surface is revealed by the FE-SEM images shown in Fig. 4. It turns out that the surface

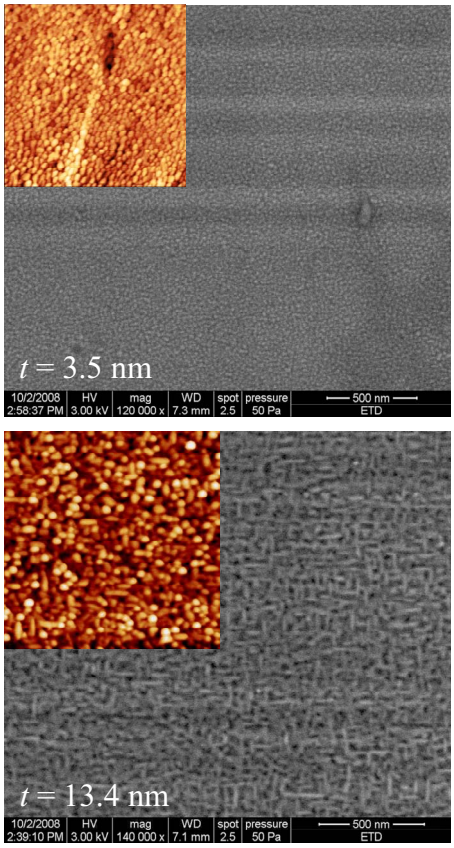

FIG. 4. (Color online) FE-SEM images of CFO films of various thickness. Insets are the corresponding AFM images.

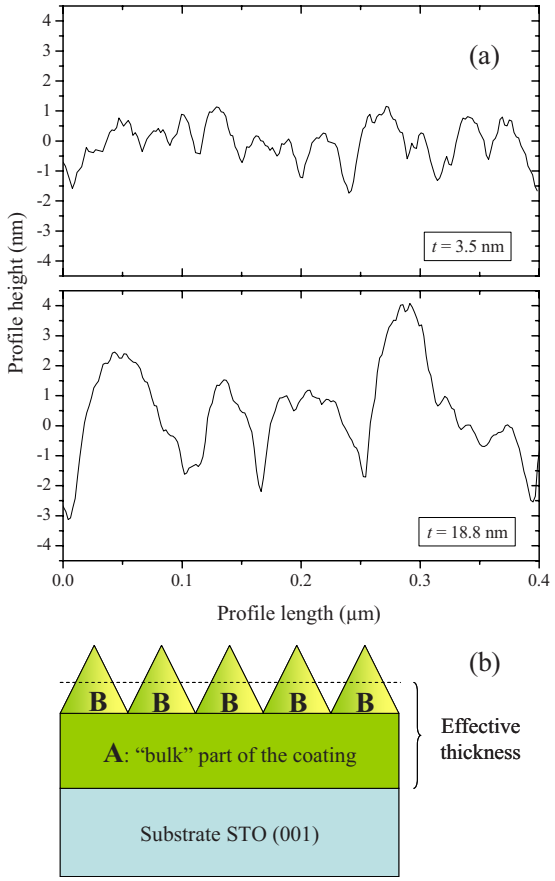

FIG. 5. (Color online) (a) AFM scan lines across the surface of CFO films of various thicknesses; (b) sketch of the observed morphology.

of the films is covered by elongated pyramidal huts objects whose height (h) increases with thickness. The objects are elongated either along the [100] or along [010] directions of the substrate. In fact, they are well visible for the thicker films but can hardly be discriminated in the thinnest one. Growth of pyramidal huts of other spinels on cubic substrates has been reported previously.[18,19] In the insets of the FE-SEM images (Fig. 4), the AFM images used to determine h of the pyramidal huts are included. In Fig. 5(a) we show AFM scan lines across the surfaces of the CFO films with t=3.5 and 18.8 nm. From these and similar scans, we deduced a mean peak-to-peak distance that we took as a measure of h. It turns out that h=4.6, 2.6, 4.9, and 6.7 nm for t=3.5, 5.2, 13.4, and 18.8 nm, respectively. In Fig. 5(b), we sketch the observed surface morphology.

The volume of these pyramidal huts can be estimated by assuming complete coverage of the film surface and using h as their average height. The relative volume (f) of pyramidal huts with respect to the total film volume is shown in Fig. 6(a) (main panel). The data in Fig. 6(a) reveal that, in spite of the increasing h when increasing t, its relative contribution to the total volume of CFO film is progressively lowered. This observation provides an important insight into the origin of the two phases we identified from the magnetization loops: phase A corresponds the continuous CFO films, and phase B represents the pyramid fraction which becomes relatively larger for the thinner films. Phase B accounts for the smaller anisotropy and coercivity, whereas phase A, representing the bulk of the films, has a larger coercivity and easy-plane magnetic anisotropy, progressively modified (reduced) by strain relaxation.

In order to verify this scenario, we have evaluated the total magnetic energy of the films when magnetized along the in-plane [100] direction, assuming to be composed of the above mentioned phases A and B. Phase A is the continuous (001)-textured $CoFe_2O_4$ magnetic film with saturation magnetization M_S and with effective anisotropy constant K_1^{eff}. Here, $K_1^{\text{eff}}=K_{\text{mc}}+K_{\text{ext}}$, where K_{mc} is the first-order magnetocrystalline anisotropy constant (considering negligibly small the higher order terms), and the extrinsic K_{ext} part includes contributions coming from the magnetoelastic anisotropy K_{me}, which results from in-plane stress and from the surface anisotropy, i.e., $K_{\text{ext}}=K_{\text{me}}+K_S$.

The data in Fig. 1(a) indicated that the basal plane is magnetically easier than the out-of-plane direction, as expected for a dominating K_{me} contribution for compressive strained films with $\lambda<0$. In any event, K_{mc} and K_{me} represent biaxial anisotropies in the (001) plane. Note that in materials with cubic symmetry such as CFO, stress anisotropy contributions have the same symmetry as magnetocrystalline anisotropy; therefore, knowing the in-plane symmetry and magnitude of the magnetic anisotropy is not sufficient to distinguish whether the biaxial anisotropy is dominated by magnetocrystalline or stress effects.[7] The shape anisotropy (with $K_{\text{dem}}=2\pi M_S^2$) induces an easy-magnetization plane which is of no relevance when comparing the in-plane $M(H)$ loops of all films.

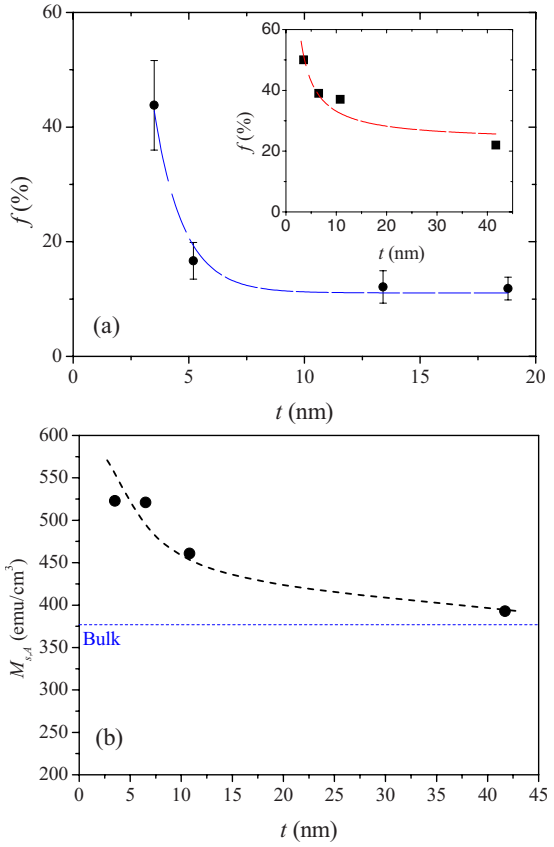

FIG. 6. (Color online) (a) Dependence on thickness of the relative volume fraction (f) of the pyramidal huts. The circles and squares are the values of f determined from the microscopy images and from the magnetization loops, respectively. (b) Saturation magnetization of the film (phase A) vs the thickness as extracted from the fits using the experimental f fraction as input parameter (dashed lines are simply guides to the eyes).

For H applied in the plane of the films, the angular dependence of the magnetic energy per unit volume of a monodomain crystallite can be written as

$$E_A = -M_S H \cos(\theta - \theta_H) + \tfrac{1}{4}K_1^{\text{eff}} \sin^2 2\theta. \quad (1)$$

Here, the first term gives the Zeeman energy, the second one is the effective in-plane biaxial anisotropy, and θ and θ_H represent the angles that M_S and H form with the [100] direction, respectively. $K_{\text{mc}}>0$ for $CoFe_2O_4$ and, since our films are under compression, K_{me} is positive as well. Therefore, K_1^{eff} is positive, being [100] and [010] the in-plane easy-magnetization orientations. As Fig. 1(b) shows, the difference between hysteresis loops traced with field applied along distinct in-plane directions is rather small; this observation, together with the long "tail" of the loops at the high-field regions (i.e., the descending and ascending branches of the loops stay close together but do not coincide for a broad field range) suggest that there is a distribution of anisotropy values. Accordingly, each film is assumed to be divided into a number of monodomains having a distribution of K_1^{eff}. For simplicity, a rectangular K_1^{eff} distribution ($\pm 50\%$) is assumed. The saturation magnetization of each sample has been estimated from the measured $M(H)$ loops in Fig. 2 and consequently used in the respective simulations.

Phase B consists of "pyramidal huts" emerging from the continuous film constituting phase A and having a height between 2.5 and 7.0 nm and lateral dimensions between 30 and 160 nm, as deduced from Figs. 4 and 5(a). The sharp change in magnetization at low field suggests that they can be best described as having in-plane uniaxial anisotropy constant, K_U. In accordance with the AFM and FE-SEM data, there are two populations of pyramidal huts, aligned along [100] and [010], and with the corresponding easy-magnetization axis along either [100] or [010] in-plane orientation. For H applied in the film's plane, the magnetic energy per unit volume of phase B can be written as

$$E_B = -\sum_{i=1,2} [M_S H \cos(\theta_i - \theta_H) + K_U \cos^2 \theta_i]. \quad (2)$$

The first term in Eq. (2) is the Zeeman energy; the second term represents the uniaxial anisotropy energy of the two pyramidal huts distributions, where $\theta_i (i=1,2)$ are the angles that the magnetization vectors of these two populations form with the respective easy axes (either [100] or [010] orientation). We assume here a Gaussian distribution of these easy directions (see the AFM and/or FE-SEM images); standard deviations of 10° from the [100] or [010] directions, respectively, were used in all simulations. The anisotropy field $2K_U/M_S$ was taken to be 1.5 kOe. This value represents the mean value of all island contributions. Such uniaxial distribution produces an in-plane hysteresis loop nearly independent of the H-orientation and a coercivity of about 0.8 kOe, in agreement with the experimental data. This magnetically soft phase is responsible for the sharp magnetization drop in the low-field region more visible in the thinnest films. This uniaxial contribution most likely originates from strain acting on pyramid edges and surfaces rather than from shape anisotropy of the elongated pyramids (the later was estimated to result in negligibly low anisotropy field).

Using this simple model, we have simulated the return section $[H \in (-H_{\text{max}}, 0)]$ of the magnetization loop of the CFO films of various thicknesses (see the solid curves in Fig. 7), by using a weighted average of phases A and B, $M/M_S = [(1-f)M_A + fM_B]/M_S$, where f is the volume fraction of phase B. Only two parameters have been allowed to vary during the fits. In Fig. 7, the field-dependent magnetization for $H \in (H_{\text{max}}, 0)$ is not depicted since, in this field region, the experimental curves are rather rounded; magnetic flux-closure domains are formed minimizing the energy that might be responsible for this behavior. This effect cannot be captured by the simple model we used.

We will first assume the saturation magnetizations of phases A and B to be equal ($M_{S,A}=M_{S,B}$) and K_1^{eff} and the relative fraction f of phase B will be determined from the fits. Alternatively, we will use the experimental values of $f(t)$ from the main panel of Fig. 6(a) in order to extract $M_{S,A}$ from the fits, assuming that the saturation magnetization of phase B is constant.

Figure 8 shows the thickness dependence of K_1^{eff}, extracted from the fits. It turns out that its value decreases as t increases (circles, top axis). As mentioned above, the observed reduction in the effective anisotropy K_1^{eff} could in principle steam from the reduction in the magnetoelastic and/or the surface contribution with increasing thickness. The magnetoelastic anisotropy of a tetragonally distorted cu-

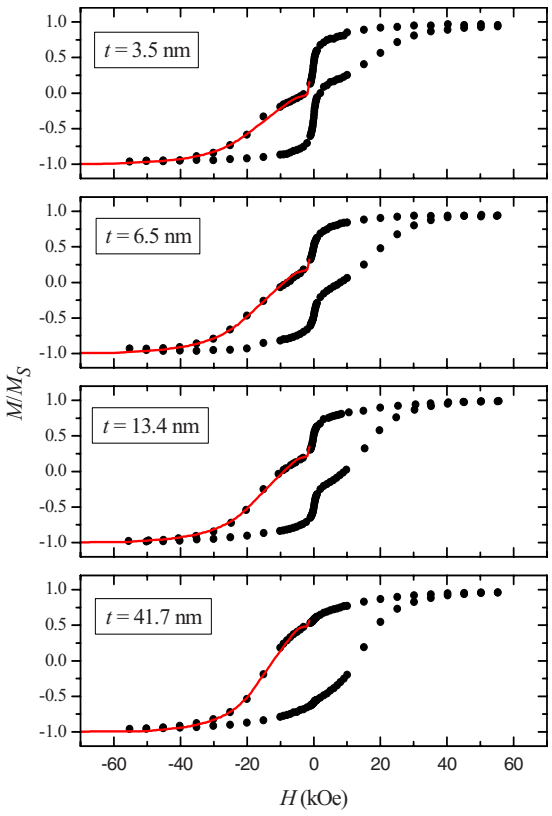

FIG. 7. (Color online) Magnetization loops of the CFO films. The solid lines across the experimental values in the second and third quadrants represent the fits of the data obtained by the two phase model.

bic lattice is given by $K_{me}=3/2[\lambda_{[100]}(C_{11}-C_{12})(\varepsilon_2-\varepsilon_1)]$, where $\lambda_{[100]}$ is the magnetostriction constant along [100], C_{11} and C_{12} are the elastic constants, and ε_2 and ε_1 are the strains which can be simply related to the strained cell parameters by the relation $(a-a_{bulk})/a_{bulk}$. As the term $(\varepsilon_2-\varepsilon_1)$ decreases with thickness, the magnetoelastic contribution to the anisotropy should also decrease. On the other hand, the surface anisotropy is known to vary with the thickness as $K_S \sim 1/t$.

In Fig. 8 (square symbols, bottom axis), we show K_1^{eff} plotted versus $1/t$. These data can be well described by the

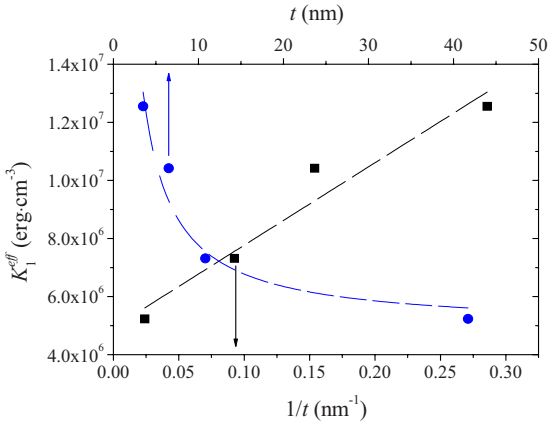

FIG. 8. (Color online) The dependence of the K_1^{eff} on thickness (circles, top axis) and on reciprocal thickness (squares, bottom). The dashed lines are intended as a guide for the eyes.

$K_1^{eff}=K_1+Q/t$, where Q ($\approx$2.8 ergs/cm^2) reflects the thickness dependence of K_1^{eff} resulting from the combined contributions of K_{me} and K_S. Using $K_{me}=3/2[\lambda_{[100]}(C_{11}-C_{12})(\varepsilon_2-\varepsilon_1)]$ and the bulk values[7,20] of $C_{11}(\approx 2.7\times10^{12}$ dyn/cm^2), $C_{12}(\approx 1.06\times10^{12}$ dyn/cm^2), and $\lambda_{[100]}(\approx -6.10^{-4})$, the magnetoelastic anisotropy constant K_{me} for the 13.4 nm thick film is estimated to be about 2.1×10^6 ergs/cm^3. The Q/t term in $K_1^{eff}(1/t)$ for the same sample is $\approx 1.9\times10^6$ ergs/cm^3 and thus we conclude that the thickness dependence of K_1^{eff} is largely dominated by the magnetoelastic effect, leaving to the surface anisotropy a minor role ($\approx$10%) on the observed decrease in K_1^{eff} with thickness.

The $f(t)$ values of the fraction of the B phase, extracted from the fits, are included in Fig. 6(a) (squares), where they can be compared with the relative volume of the pyramidal huts evaluated from the AFM images (circles). The agreement between both sets of data is rather good.

We turn now to the alternative fitting procedure of imposing the experimentally estimated fraction f of pyramids from Fig. 6(a) to extract the saturation magnetization of the film (phase A) and K_1^{eff} as a function of the thickness. We obtained a (constant) saturation magnetization of phase B of about 523 emu/cm^3 and a gradually decreasing $M_{S,A}$ of the film as its thickness increases [Fig. 6(b)]. The thickness dependence of the corresponding anisotropy K_1^{eff}, logically, mimics that of $M_{S,A}$ thus also lowering as a function of t. This observation would support earlier findings indicating that the magnetization of spinel films gradually decreases with increasing thickness, approaching the bulk value.[17] Note that since the measured magnetization is the product function of the relative concentration of a phase by its saturation magnetization, the fits cannot distinguish between these two scenarios.

Therefore, it follows that the magnetization of epitaxial CFO‖(001)STO films is controlled by contributions coming from (i) the epitaxial strain that induces a compression in the basal plane producing an easy-plane with biaxial anisotropy in the bulk of the CFO film, and (ii) the contribution of a collection of CFO pyramidal huts that protruded from the surface of the CFO. This model shed light on the characteristic double-step behavior observed in the magnetization hysteresis loops of ferrimagnetic spinels on (001)-textured substrates. As shown here, the ultimate reason is the existence of a collection of well-defined outgrows at the surface of the films. We would like to emphasize that the frequent observation of this unusual shape of the magnetization loop suggests that the presence of two magnetic CFO phases could be a common trend in most epitaxial CFO films. In fact, we have shown earlier[18] that, under appropriate conditions, the growth of spinels on cubic (001)-textured substrates can lead to a well-defined distribution of pyramidal huts, as a result of the lower surface energy of the exposed (111)CFO faces with respect to the (001)CFO surface that an epitaxial and atomically flat CFO layer on (001)STO would require. A way to circumvent this intrinsic difficulty could be the growth of epitaxial CFO layers on (111)-textured substrates as this would allow stabilizing free surfaces of lower specific surface energy. We have verified that this is the case.[21]

Finally, the shape of the out-of-plane magnetization

curves (Fig. 1(b)) indicates that the maximum applied field (≈48 kOe) is not sufficient to provide a high-field region where the ascending and descending branches of the loops coincide. Consequently, it was not possible to obtain the anisotropy parameters from such simulations and to cross-check them with those used for the in-plane fittings. However, it is clear from Fig. 1 that the basal plane is an easier plane as the out-of-plane curves show very small remnant magnetization and coercivity for all t.

In conclusion, we have disclosed the microscopic origin of the anomalous behavior of (001)CFO films. We have shown that it is intimately related to the microstructure of the films which in turn results from the balancing of different energy contributions during film growth. These effects are particularly relevant here as the growth of (001) spinel oxides on (001) perovskites imply strong differences of free energy surfaces. It thus follows that understanding the magnetic anisotropy of spinel thin films requires a detailed control of the film structure (strains) as well as its microstructure, being the surface morphology particularly relevant for nanometric thin films as required in advanced applications, such as spin filters or others.

ACKNOWLEDGMENTS

Financial support from the Ministerio de Ciencia e Innovación of the Spanish Government Projects (Project Nos. MAT2008-06761-C03 and NANOSELECT CSD2007-00041) and from the European Union [Project No. MaCoMuFi (FP6-03321) and FEDER] is acknowledged.

[1]U. Lüders, M. Bibes, K. Bouzehouane, E. Jaquet, J.-P. Contour, S. Fusil, J.-F. Bobo, J. Fontcuberta, A. Barthélémy, and A. Fert, Appl. Phys. Lett. **88**, 082505 (2006).
[2]M. Gajek, M. Bibes, S. Fusil, K. Bouzehouane, J. Fontcuberta, A. Barthélémy, and A. Fert, Nature Mater. **6**, 296 (2007); M. Gajeck, M. Bibes, A. Barthélémy, K. Bouzehouane, S. Fusil, M. Varela, J. Fontcuberta, and A. Fert, Phys. Rev. B **72**, 020406(R) (2005).
[3]M. G. Chapline and S. X. Wang, Phys. Rev. B **74**, 014418 (2006).
[4]A. V. Ramos, M.-J. Guittet, J.-B. Moussy, R. Mattana, C. Deranlot, F. Petroff, and C. Gatel, Appl. Phys. Lett. **91**, 122107 (2007).
[5]B.B. Nelson-Cheeseman, R. V. Chopdekar, L. M. B. Allredge, J. S. Bettinger, E. Arenholz, and Y. Suzuki, Phys. Rev. B **76**, 220410(R) (2007).
[6]H. Zheng, J. Wang, S. E. Lofland, Z. Ma, L. Mohaddes-Ardabili, T. Zhao, L. Salamanca-Riba, S. R. Shinde, S. B. Ogale, F. Bai, D. Viehland, Y. Jia, D. G. Schlom, M. Wuttig, A. Roytburd, and R. Ramesh, Science **303**, 661 (2004).
[7]Y. Suzuki, G. Hu, R. B. van Dover, and R. J. Cava, J. Magn. Magn. Mater. **191**, 1 (1999); Y. Suzuki, R. B. van Dover, E. M. Gyorgy, J. M. Phillips, V. Korenivski, D. J. Werder, C. H. Chen, R. J. Cava, J. J. Krajewski, W. F. Peck, Jr., and K. B. Do, Appl. Phys. Lett. **68**, 714 (1996).
[8]W. Huang, J. Zhu, H. Z. Zeng, X. H. Wei, Y. Zhang, and Y. R. Li, Appl. Phys. Lett. **89**, 262506 (2006); W. Huang, L. X. Zhou, H. Z. Zeng, X. H. Wei, J. Zhu, Y. Zhang, and Y. R. Li, J. Cryst. Growth **300**, 426 (2007).
[9]P. D. Thang, G. Rijnders, and D. H. A. Blank, J. Magn. Magn. Mater. **310**, 2621 (2007).
[10]L. Horng, G. Chern, M. C. Chen, P. C. Kang, and D. S. Lee, J. Magn. Magn. Mater. **270**, 389 (2004).
[11]P. C. Dorsey, P. Lubitz, D. B. Chrisey, and J. S. Horwitz, J. Appl. Phys. **79**, 6338 (1996).
[12]S. A. Chambers, R. F. C. Farrow, S. Maat, M. F. Toney, L. Folks, J. G. Catalano, T. P. Trainor, and G. E. Brown, Jr., J. Magn. Magn. Mater. **246**, 124 (2002).
[13]A. Lisfi, C. M. Williams, L. T. Nguyen, J. C. Lodder, A. Coleman, H. Corcoran, A. Johnson, P. Chang, A. Kumar, and W. Morgan, Phys. Rev. B **76**, 054405 (2007).
[14]S. Xie, J. Cheng, B. W. Wessels, and V. P. Dravid, Appl. Phys. Lett. **93**, 181901 (2008).
[15]D.-X. Chen, E. Pardo, and A. Sanchez, IEEE Trans. Magn. **38**, 1742 (2002).
[16]D. T. Margulies, F. T. Parker, M. L. Rudee, F. E. Spada, J. N. Chapman, P. R. Aitchison, and A. E. Berkowitz, Phys. Rev. Lett. **79**, 5162 (1997).
[17]U. Lüders, M. Bibes, J.-F. Bobo, M. Cantoni, R. Bertacco, and J. Fontcuberta, Phys. Rev. B **71**, 134419 (2005); F. Rigato, S. Estradé, J. Arbiol, F. Peiró, U. Lüders, X. Martí, F. Sánchez, and J. Fontcuberta, Mater. Sci. Eng., B **144**, 43 (2007).
[18]U. Lüders, F. Sánchez, and J. Fontcuberta, Phys. Rev. B **70**, 045403 (2004).
[19]In Ref. 18, pyramidal huts in thick spinel films were found to be oriented along the [110] directions.
[20]M. D. Sturge, E. M. Gyorgy, R. C. LeCraw, and J. P. Remeika, Phys. Rev. **180**, 413 (1969).
[21]F. Rigato, M. Foerster, J. Fontcuberta (unpublished).